Asociación Argentina
de Mecánica Computacional

Mecánica Computacional Vol XXIX, págs. 5953-5960 (artículo completo)
Eduardo Dvorkin, Marcela Goldschmit, Mario Storti (Eds.)
Buenos Aires, Argentina, 15-18 Noviembre 2010

INFLUENCE OF INLET CONDITIONS IN WALL SHEAR STRESS DISTRIBUTIONS OF LEFT CORONARY ARTERIES IN PATIENT-SPECIFIC SIMULATIONS

Fernando P. Salvucci[a], Carlos A. Perazzo[b], Sabina Salles[a], Juan G. Barra[c] and Ricardo L. Armentano[a]

[a]*Departamento de Electrónica,Facultad de Ingeniería y Ciencias Exactas y Naturales, Universidad Favaloro, Buenos Aires, Argentina, fsalvucci@favaloro.edu.ar*

[b]*Departamento de Física y Química, Universidad Favaloro, Buenos Aires, Argentina, cperazzo@favaloro.edu.ar*

[c]*Departamento de Fisiología, Universidad Favaloro, Buenos Aires, Argentina, jgbarra@favaloro.edu.ar*

Keywords: Coronary Arteries, Finite Elements, Atherosclerosis.

Abstract. The left coronary artery (LCA) is one of the most important sites of atherosclerotic plaque formation and its progression may lead to stroke. It is accepted that the location of atherosclerotic plaques is correlated with sites subjected to low abnormal values of wall shear stress (WSS). However, little is known about flow conditions at the inlet of the LCA, a factor difficult to determine in common clinic studies and which in turn may be determinant in the WSS distribution along the LCA. The purpose of this work is to investigate numerically the role of the flow inlet conditions of the LCA in the consequent WSS distribution in a proposed patient-specific method.

A three-dimensional model of the LCA of a healthy patient was reconstructed based on a computer tomography (CT) study. A finite element volume mesh was constructed and blood flow trough it was modeled with the finite element method. Five simulations with different inlet conditions were performed: (S1) a surface normal parabolic velocity profile, (S2) a surface normal planar velocity profile, (S3) a surface normal Dean's profile, (S4) a parabolic profile with the incidence direction being the bisectrix of aorta and ostium directions and (S5) a parabolic profile with a random incidence direction. WSS distributions were computed with later postprocessing.

Results showed in all cases that the WSS distribution pattern did not differ between simulations. Being S1 the standard inlet condition, the other simulations showed some differences in WSS values, in all cases acceptable. S2 showed a mean WSS difference of 15%. S3 showed a mean WSS difference of 6%, whereas S4 and S5 of 32% and 38% respectively. In all cases, the difference in each point of the mesh was proportional to the WSS value, being more negligible the difference in the regions of interest (regions of low WSS). Also, the differences were concentrated in the first segment of the mesh where the flow developed.

This work shows that WSS distribution pattern in the LCA does not depend of the inlet condition. Although the absolute values of WSS may be slightly different depending on the assumed condition (being the incidence direction the feature that most affected them), the objective is to localize the regions of low WSS, despite its absolute value. These results show that what is really determinant in WSS distribution is the particular geometry of the patient LCA.

1 INTRODUCTION

Atherosclerosis is the leading cause of mortality and morbidity in the western world. It is a chronic, inflammatory, fibroproliferative disease of arteries (Chatzizisis et al., 2007). Although the entire vasculature is exposed to the atherogenic effects of the systemic risk factors, atherosclerotic lesions form at specific regions of the arterial tree, an observation that has led to the "geometric risk factor" hypothesis for atherogenesis (Myers et al., 2001). The essence of this geometrical factor relies in the local hemodynamic forces. In particular, the major hemodynamic factor that seems to play an important role in atherogenesis and disease progression is wall shear stress (WSS) (Davies, 2009; Caro, 2009; Steinman, 2002; Katritsis et al., 2007).

WSS expresses the force per unit area exerted by the blood in motion on the internal wall of the artery in the direction of the local tangent plane. It is determined in each site of a vascular segment by the flow conditions and the particular geometry of the segment. Nowadays, it is widely accepted that the location of atherosclerotic plaques is correlated with sites subjected to low abnormal values of WSS (Davies, 2009; Caro, 2009; Steinman, 2002).

In particular, the left coronary artery (LCA) is a common and one of the most important site of atherosclerotic plaque formation, since the progression of the disease or a vulnerable plaque may induce to stroke. We have previously proposed a patient-specific method (Salvucci et al., 2010) to study blood flow in real LCA geometries, combining Computer Tomography (CT) studies, digital image processing techniques and the Finite Element Method (FEM). This method provides the WSS distribution along the LCA.

A factor difficult to determine in common clinic studies and that remains unclear is the flow conditions at the inlet of the LCA, that is, the ostium velocity profile, which is determined by the interaction of aortic and coronary hemodynamics (Figure 1A). Being these flow conditions still not well characterized, its influence in the flow pattern along the LCA and its WSS distribution is an issue to be clarified specially when trying to set up a patient-specific method.

The objective of this work is to investigate the influence of the inlet flow conditions of the LCA in the consequent WSS distributions with the proposed patient-specific method. For this purpose, FEM simulations of blood flow in a real LCA geometry with different inlet velocity profiles were performed, with the later comparison of the respective WSS patterns.

2 MATERIALS AND METHODS

2.1 3D Model Construction

A 3D model of the LCA of an asymptomatic and healthy patient was constructed based on a multislice CT scan performed in the Hospital Universitario, Fundación Favaloro, Buenos Aires, Argentina. The scan was done using a 64-row MSCT scanner (Aquilion 64, Toshiba, Japan). Images were acquired during diastole by means of ECG-gating using a 400–960 ms time window in order to reduce motion facts. Transaxial images were reconstructed with 0.415 mm slice thickness and 0.3 mm increments.

A detailed explanation of the model generation is described elsewhere (Salvucci et al., 2010). Briefly, a sequence 40 consecutive images (512 by 512 pixels, 256 gray levels) were imported from the scan in order to reconstruct the whole LCA, beginning in the ostium, including the left main artery (LM), the main branch, the left circumflex (LCX) and left anterior descending (LAD) arteries until an important secondary branch in any of them appeared (Figure 1B). In each slice, automatic segmentation of the vessels lumen was

performed. Next, a 3D surface triangulization based on the detected lumen was done. The three-dimensional skeleton of the vessels was obtained with a sequential 3D thinning algorithm (Palágyi et al., 2001). The surface was then cut with consecutive normal planes following the vessels skeleton in each point to obtain the contours of the vessels. These contours were parameterized as B-Splines. Finally, the contours were imported into a CAD software where a NURBS surface was constructed with them in order to achieve the final 3D model of the LCA (Figure 2A).

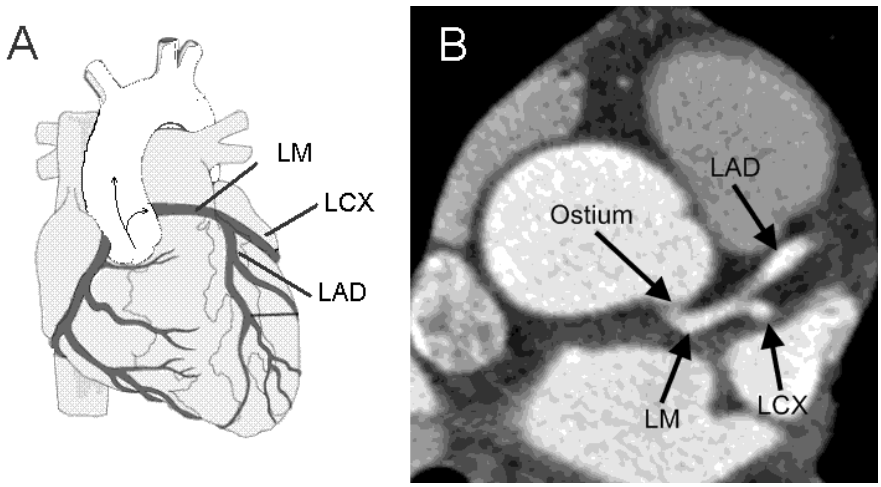

Figure 1: Panel A shows LCA anatomy, note that inflow in the ostium deviates from aortic flow. Panel B is an example of one CT slice image used for the LCA reconstruction. These images permit to distinguish the coronary ostium, the left main artery (LM), the left anterior descending (LAD) and left circumflex (LCX) branches.

2.2 Volume Mesh Generation

The 3D surface model was discretized into finite elements with the open-source software Netgen (hp-FEM), obtaining the initial unstructured mesh. A posterior refinement of the near-wall region with prism elements was performed with the open-source software enGrid (enGits). The final volume mesh (Figure 2B) consisted of 222200 elements.

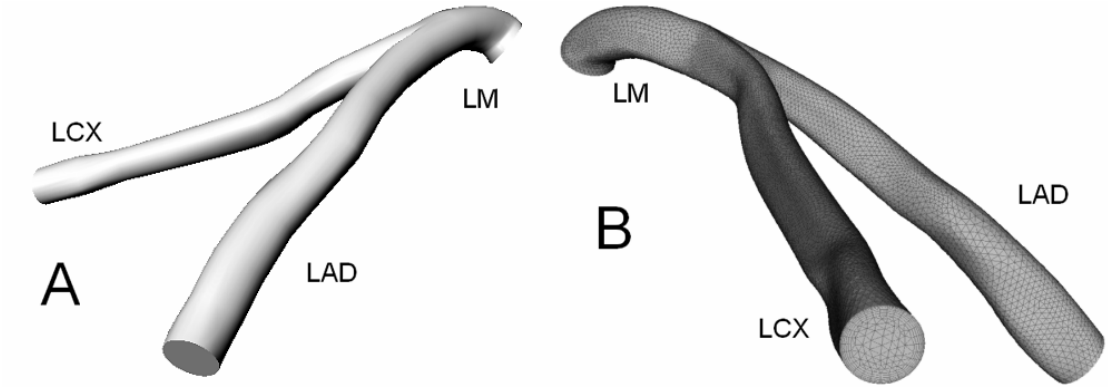

Figure 2: 3D NURBS model (panel A) and the corresponding finite element mesh (panel B) of LCA, showing the main artery (LM), the left anterior descending (LAD) and left circumflex (LCX) branches.

2.3 Computational Simulations

Blood flow through the LCA was simulated using the finite element code OpenFoam (OpenCFD Ltd.). A SIMPLE solver was used to solve the governing three-dimensional Navier-Stokes equations to obtain the velocity vector $\vec{v}$ and pressure p in every point of the mesh. Flow was assumed to be steady and laminar. Blood was considered as a homogeneous Newtonian fluid with a dynamic viscosity of μ=0.0035 Pa×s and incompressible with a density of ρ=1050 kg/m^3. The vessel wall was modeled as rigid.

Five simulations were performed with different inlet velocity profiles. The two first profiles utilized correspond to standard inlet velocity profiles for blood flow simulations (Farmakis et al., 2004; Myers et al., 2001; Moyle et al., 2006):

(S1): surface normal parabolic velocity profile

(S2): surface normal planar velocity profile

In order to make the situation more realistic and take into account the nature of the flow entering the ostium from the aorta (Figure 1A), two profiles were proposed:

(S3): surface normal Dean-type profile

(S4): parabolic profile with the incidence direction being the bisectrix of aorta and ostium directions

The more unfavorable situation was considering a parabolic profile but with an incidence direction selected randomly:

(S5): parabolic profile with a random incidence direction

The assumption of a fully developed Dean-type velocity profile seemed to be the more realistic one, considering that a portion of flow form the aorta deviates in a curved manner into the ostium. This profile (Figure 3) exhibits a pair of symmetric counter-rotating Dean-type secondary vortices and an offset axial profile, shifted toward the outer wall of curvature (Myers et al., 2001; Johnson and Kamm, 1986) (Eq 1).

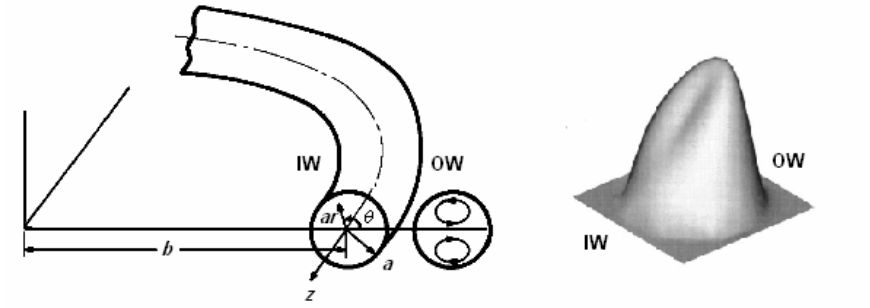

Figure 3: Fully Developed Dean-type profile, exhibiting the symmetric counter-rotating vortices and the shifted profile. OW and IW are the outer wall and inner wall of curvature respectively.

$$
\begin{aligned}
D_n &= \left(\frac{a}{b}\right)^{\frac{1}{2}} \cdot Re \\
V_z &= V_{\max}\left[D_n{}^2 g(r)\cos(\theta) + 1 - \left(\frac{r}{a}\right)^2 \right] \\
V_r &= \frac{\upsilon}{r \cdot a} D_n{}^2 f(r)\cos(\theta) \\
V_z &= -\frac{\upsilon}{a} D_n{}^2 \frac{df(r)}{dr}\sin(\theta)
\end{aligned}
\tag{1}
$$

Where a is the vessels radius, b the curvature radius, D_n the Dean's number, Re the Reynolds number, υ the blood kinematic viscosity, and $f(r)$ and $g(r)$ polynomial functions of r. For S3, a was set as the ostium radius, b the aorta radius (D_n = 10.25), and the plane of curvature the one determined by the aorta and the ostium direction vectors. For this purpose, the first segment of the aorta was reconstructed and its skeleton obtained. The 3D angle measured between the aorta and the ostium direction vectors was 86.52°.

For S4, the bisectrix direction between the aorta and ostium direction vectors was calculated, and used to impose the parabolic profile. The 3D measured angle between this incidence direction and ostium direction was 43.26°.

Finally, for S5, the 3D measured angle between the randomly selected incidence direction and the ostium direction resulted of 92°, an unrealistic situation.

In all cases, pressure was set to zero at the LCX outlet. Flow splitting in the principal branch was set according to Murray's cubic law (Soulis et al., 2006), imposing then a parabolic profile with the calculated velocity in the LAD outlet, and a free traction condition in the other. Velocity was set to zero at the vessels walls according to the non-slip condition.

After the simulations were performed, WSS was computed from the gradients of the velocity fields near the wall:

$$
WSS = \left| \mu \frac{d\vec{v}}{d\vec{n}} \right| \tag{2}
$$

where $\vec{n}$ is the vector normal to the wall in each point.

3 RESULTS

The five simulations showed similar flow patterns, with the main differences concentrated in the first segment of LM, where the flow develops. A qualitative comparison of the WSS distribution for all the simulations is shown in Figures 4 and 5. The WSS pattern was similar in the five simulations, concentrating the main differences also in the first segment of LM. In all cases, low WSS regions were found in the walls opposite to the flow divider in the bifurcation, as expected (Caro, 2009; Soulis et al., 2006; Katritzis et al., 2007). Also, a low WSS region was found in the inferior wall of LM, consistent with the fact that its curvature shifts the velocity profile into the upper wall of the segment. Other low WSS regions were found, principally in the LAD artery.

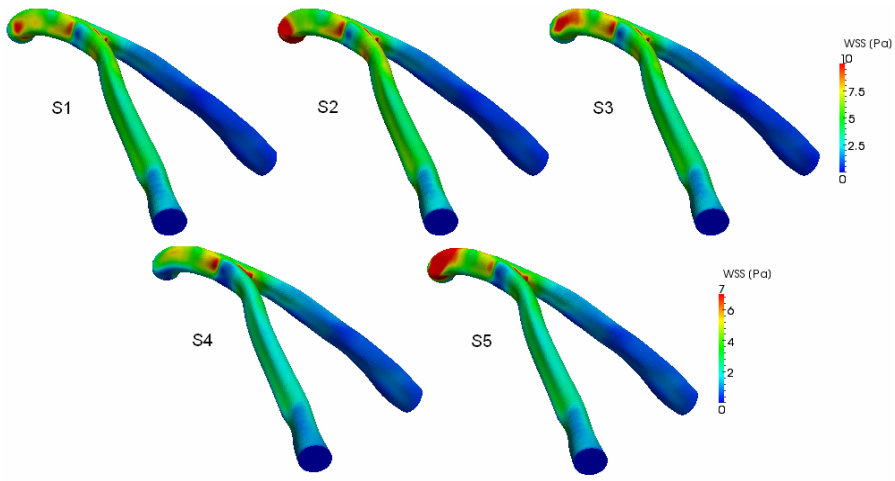

Figure 4: WSS plot along the LCA for the five simulations. Note the low WSS region in LCX opposite to the bifurcation.

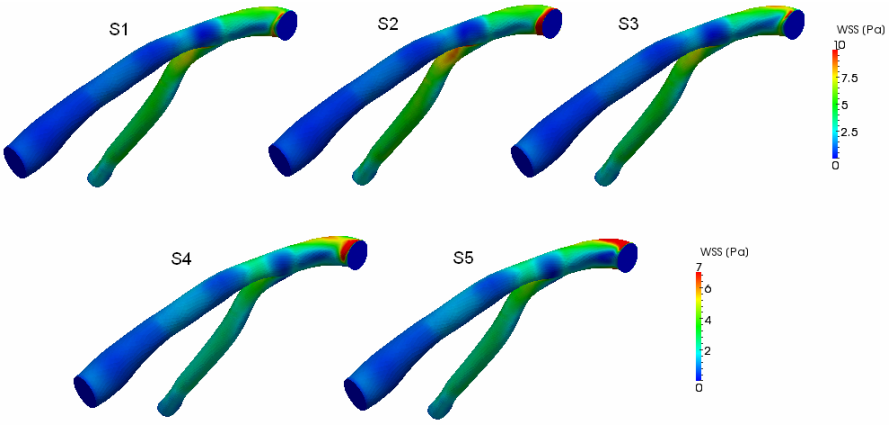

Figure 5: WSS plot along the LCA for the five simulations. Note the low WSS regions in the inferior wall of LM, the beginning of LAD opposite to the bifurcation and the other regions through LAD.

The differences of WSS values in each point of the mesh for S2-S5 with respect to S1 (considered the parabolic profile as the standard inlet profile used in simulations) were computed. S2 showed a mean WSS difference of 15%, S3 of 6%, whereas S4 and S5 of 38% and 32% respectively. In all cases, these differences were concentrated in the first segment of LM, something expected since it is just in this region that the different profiles would develop according to the vessels geometry.

Finally, the WSS differences in each point of the mesh were proportional to its WSS value, being more negligible in the regions of interest (regions of low WSS). Figure 6 shows an example of this for the case of S2.

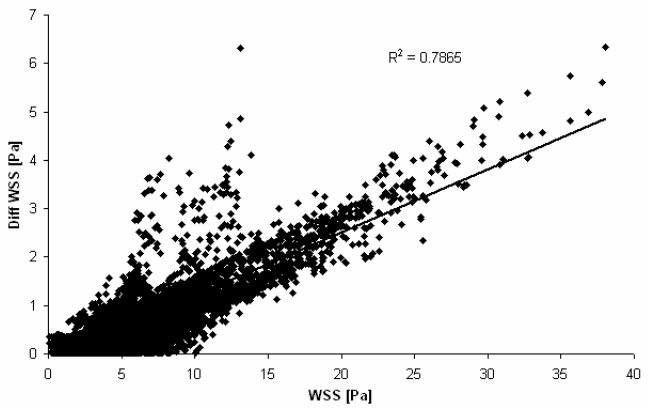

Figure 6: Difference in WSS between the simulation with planar inlet profile (S2) and the simulation with parabolic inlet profile (S1) as a function of WSS value in S1.

4 DISCUSSION

The aim of this work was to investigate the influence of the inlet profile of the LCA on the developed flow patterns, and specially, on the WSS distributions, in order to advance in the concretion of a patient-specific method for the evaluation and study of atherosclerosis in coronary circulation. The importance of this study relies in the difficulty to determine in practice the velocity profile developed in the ostium of LCA for a given patient, due in part to the complex nature of ostium flow and the great intra-patient variability of coronary geometry, and to the absence of a non-invasive technique for its measurement in clinic practice.

Our results show that for all of the five proposed profiles, WSS distributions along the LCA were similar. The localization of the low WSS regions was the same for all the simulations, and coincided with was expected.

The biggest differences were found when changing the incidence direction of flow, for S4 and S5. However, these were the more unrealistic and unfavorable conditions.

In all cases, the main differences were found in the first segment of LM, a region of not many interest due to the considerable distance to the branching, since experimental evidence show that atherosclerotic plaques appear principally in LAD and LCX, in the branching region and distal to it (Caro, 2009; Rodriguez-Granillo et al., 2007; Vogl et al., 2002).

Additionally, in all simulations, the differences of WSS due to the different inlet profile assumed were proportional to the WSS value in each point. Considering that the regions of interest correspond to those with low WSS values (Caro, 2009; Davies, 2009; Katritzis et al., 2007), this also suggests that the differences are negligible.

5 CONCLUSION

This work shows that the wall shear stress distribution in the left coronary artery does not depend of the inlet velocity profile present in the ostium. Although the absolute values of wall shear stress may be slightly different depending on the assumed inlet condition (being the incidence direction the feature that most affected them), the objective is to localize the regions of low wall shear stress, despite its absolute value.

Our results confirm the hypothesis that the truly determinant feature in patient-specific simulations is the arterial geometry, which determines the flow and wall shear stress patterns developed.

REFERENCES

Caro C.G., Discovery of the role of wall shear in atherosclerosis. *Arterioscler Thromb Vasc Biol*, 29: 158–161, 2009.

Chatzizisis Y.S., Coskun A.U., Jonas M., Edelman E.R., Feldman C.L. and Stone P.H., Role of endothelial shear stress in the natural history of coronary atherosclerosis and vascular remodeling: molecular, cellular, and vascular behavior. *J Am Coll Cardiol*, 49: 2379–2393, 2007.

Davies P.F., Hemodynamic shear stress and the endothelium in cardiovascular pathophysiology. *Nat Clin Pract Cardiovasc Med*, 6: 16–26, 2009.

Farmakis T.M., Soulis J.V., Giannoglou G.D., Zioupos G.J. and Louridas G.E., Wall shear stress gradient topography in the normal left coronary arterial tree: possible implications for atherogenesis. *Curr Med Res Opin*, 20: 587–596, 2004.

Johnson M. and Kamm R.D., Numerical studies of steady flow dispersion at low Dean number in a gently curving tube. *J Fluid Mech*, 172: 329–345, 1986.

Katritsis D., Kaiktsis L., Chaniotis A., Pantos J., Efstathopoulos E.P. and Marmarelis V., Wall shear stress: theoretical considerations and methods of measurement. *Prog Cardiovasc Dis*, 5: 113–119, 2007.

Myers J.G., Moore J.A., Ojha M., Johnston K.W. and Ethier C.R., Factors influencing blood flow patterns in the human right coronary artery. *Ann Biomed Eng*, 29: 109–120, 2001.

Moyle K.R., Antiga L. and Steinman D.A., Inlet conditions for image-based CFD models of the carotid bifurcation: is it reasonable to assume fully developed flow? *J Biomech Eng,* 128: 371–379, 2006.

Palágyi K., Sorantin E., Balogh E., Kuba A., Halmai C., Erdohelyi B., and Hausegger K., A sequential 3D thinning algorithm and its medical applications, *Lect Notes Comput Sci*, 2082: 409–415, 2001.

Rodriguez-Granillo G.A., Rosales M.A., Degrossi E., Durbano I. and Rodríguez A.E., Multislice CT coronary angiography for the detection of burden, morphology and distribution of atherosclerotic plaques in the left main bifurcation. *Int J Cardiovasc Imaging*, 23: 389–392, 2007.

Salvucci F.P., Perazzo C.A., Gurfinkel E., Armentano R.L. and Barra J.G., A patient-specific method for the evaluation of wall shear stress in human coronary arteries. *Conf Proc IEEE Eng Med Biol Soc*, 3788–3791, 2010.

Soulis J.V., Farmakis T.M., Giannoglou G.D., Louridas G.E., Wall shear stress in normal left coronary artery tree. *J Biomech*, 39: 742–749, 2006.

Steinman D.A., Image-based computational fluid dynamics modeling in realistic arterial geometries. *Ann Biomed Eng*, 30: 483–497, 2002.

Vogl T.J., Abolmaali N.D., Diebold T., Engelmann K., Ay M., Dogan S., Wimmer-Greinecker G., Moritz A., and Herzog C., Techniques for the detection of coronary atherosclerosis: multi-detector row CT coronary angiography. *Radiology*, 223: 212–220, 2002.